2019

The temporal-spatial evolution of electron dynamics induced by femtosecond double pulses

Changji Pan
Beijing Institute of Technology

Lan Jiang
Beijing Institute of Technology

Jingya Sun
Beijing Institute of Technology, sjy@bit.edu.cn

Qingsong Wang
Beijing Institute of Technology

Feifei Wang
Beijing Institute of Technology

See next page for additional authors

Authors
Changji Pan, Lan Jiang, Jingya Sun, Qingsong Wang, Feifei Wang, and Yongfeng Lu

The temporal-spatial evolution of electron dynamics induced by femtosecond double pulses

Changji Pan,[1] Lan Jiang,[1] Jingya Sun,[1] Qingsong Wang,[1] Feifei Wang,[1] and Yongfeng Lu[2]

1 Laser Micro/Nano-Fabrication Laboratory, School of Mechanical Engineering, Beijing Institute of Technology, Beijing, People's Republic of China
2 Department of Electrical Engineering, University of Nebraska-Lincoln, Lincoln, NE 68588-0511, United States of America

Corresponding author — Jingya Sun, *email* sjy@bit.edu.cn

Abstract

The temporal and spatial electron dynamics were investigated under irradiation of temporally shaped femtosecond double pulses. Filament split was observed upon arrival of the second pulse, which was attributed to the emergence of transient high-reflective surface induced by the first pulse. The electron density analysis showed that the total deposition energy of double pulses case was generally higher than that of single pulse case. Particularly, the maximum deposition energy was obtained at 350 fs separation time of double pulses. The results of our experiment demonstrated optimization of energy deposition efficiency by temporally shaping laser pulses, which will benefit the fabrication process.

High-power ultrafast laser pulse induced electron plasma and filamentation are flourishing fields of nonlinear optics because of its numerous applications in waveguide writing,[1,2] terahertz wave generation,[3–5] fiber fabrication,[6]

Published in *Japanese Journal of Applied Physics* 58 (2019), 030901.
doi 10.7567/1347-4065/ab00a8

Submitted January 14, 2019; accepted January 22, 2019; published February 4, 2019.

and micro/nano processing.[7–10] Various aspects of filaments induced by single ultrashort laser pulses have been widely investigated, such as peak intensity,[11–13] filament length,[14,15] and deposition energy.[16,17] Recently, temporally and spatially shaped femtosecond laser pulses have emerged as powerful tools in femtosecond laser fabrication.[18–22] It aims to improve the material processing results by controlling electron dynamics during the excitation processes. Electron dynamics excited by shaped pulses differs from that excited by a normal Gaussian single pulse and is strongly dependent on the temporal and spatial energy distribution of pulses.[18,23] Therefore, Ref. 18 proposed a systemic fabrication method based on electron dynamics control by shaping femtosecond laser pulses, and they obtained exciting results in terms of both fabrication precision and efficiency. For instance, the fabrication efficiency can be enhanced 56 fold, and the aspect-ratio can be enhanced 3 fold. Reference 24 also realized manipulation of breakdown and thus control of the initial steps of laser processing of wide bandgap materials through temporally tailed femtosecond pulses, whose results were interpreted by numerical simulation in terms of free electron density generation.

For the extremely fast process of electron dynamics evolution, the femtosecond laser pump–probe technique is an effective tool for detecting electron dynamics during laser pulses irradiation. However, most studies have been confined to electron dynamics induced by a single pulse, while research into the evolution of electron dynamics excited by shaped pulses, such as double pulses, is scarce.[25] Indeed, in order to deeply reveal the effect of shaped femtosecond laser pulses on electron dynamics, the pump and probe pulses should be functionally separated so that the electron dynamics can be recorded within whole duration of shaped pump pulses. Direct observation of electron dynamics over shaped pulses duration can be obtained by varying the pulse separation time from zero to hundreds of femtoseconds.

In this study, we conducted a pump–probe experiment based on double pump pulses excitation for wide bandgap material (fused silica). The evolution of electron dynamics was recorded at a high temporal and spatial resolution. Filament split was observed on arrival of the second pump pulse, but it was not observed for single pulse case. However, the split disappeared as the time between double pump pulses became larger. The electron density distribution was analyzed both in and near the center of the filaments to account for the coupled energy distribution of the laser pulses. The total deposition energy was also estimated and compared for double pulses with different separation times and single pulse, which revealed the potential efficiency improvements from using temporally shaped femtosecond laser pulses.

A schematic of the experimental setup is shown in Fig. 1. The laser pulse generated from a commercial femtosecond laser system (Spectra-Physics

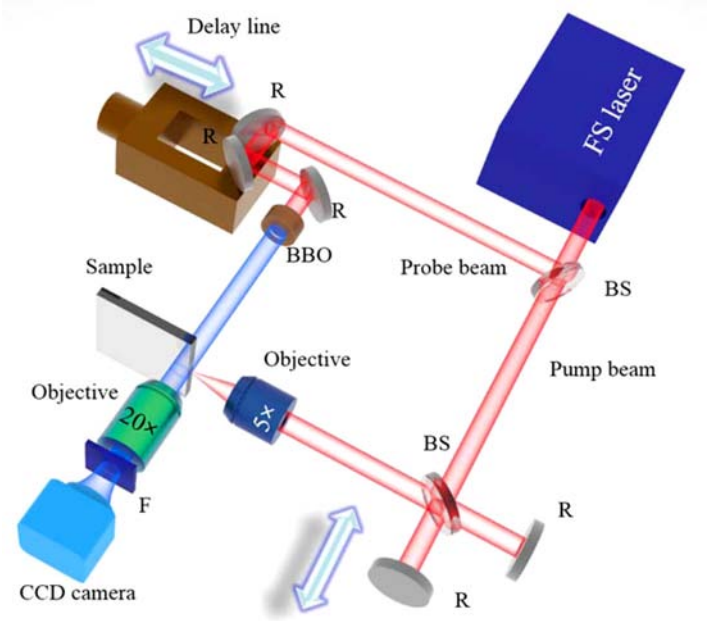

Fig. 1. Schematic of the experimental setup. F, filter; R, reflector; BS, beam splitter; BBO, beta barium borate.

Spitfire Ace) with a wavelength (λ) of 800 nm and pulse duration of 35 fs that was split into two pulses by a beam splitter. One pulse was guided into a Michelson interferometer to generate two subpulses, which served as the pump pulses and were focused onto the surface of the sample by an objective (5×, NA= 0.15, Olympus Inc.). In this case, the focus radius can be estimated as 3.3 μm according to Rayleigh Criterion. The other pulse passed through an optical delay line, and its frequency was doubled by a beta barium borate crystal to generate a 400 nm pulse, which served as the probe pulse. The probe pulse was then adjusted perpendicularly to illuminate the excited region with a precisely designed delay time by using the optical delay line. Finally, the transmitted shadowgraph of plasma was imaged onto a charge-coupled device (CCD) using another objective (20×, NA=0.45, Olympus Inc.). A 400 nm band-pass filter was mounted in front of the CCD camera to exclude the influence of pump pulses. The separation time between the double pump pulses was controlled by changing the position of a reflector, which was mounted on a linear positioner in an arm of the Michelson interferometer. The sample used in the experiment was a 10mm×10mm×1 mm piece of fused silica with four polished surfaces. To initiate the experiment, the zero-delay time was defined as the first appearance of filament at the sample edge. The shadowgraph images of the sample were recorded by the CCD camera both in the case of non-irradiation and irradiation with pump

pulses. Thus, the transmissivity was calculated on the basis of these shadowgraph images, the method is detailed in the Ref. 26. The intensity of the probe pulse was assumed to exponentially decay when it passed through the filament region. The absorption depth of the probe pulse was estimated from the mean diameter of the filament in the recorded images. By using the Drude model,[27] we estimated the electron density based on the measured transmissivity. The electron collision time for the Drude model was chosen as 0.2 fs in this experiment. In order to avoid confusion, the probe delay time was denoted by t to distinguish it from the pump separation time (t_s).

Figure 2(a) shows two-dimensional (2D) transmission mapping and the electron density evolution in the center of filaments induced by double pump pulses with a time separation of 200 fs. The transmissivity of the excited region is 2D-mapped with a color bar. As shown in the right column of Fig. 2(a), the first pump pulse can induce a filament with low transmissivity inside fused silica (shown as t = 100– 400 fs). The low transmissivity was attributed to strong absorption of the probe pulse by the pump laser induced plasma. Based on the transmissivity mapping, the electron density distribution in the center of the filament was calculated with a delay time from 100 to 800 fs, and it is shown as the left column in Fig. 2(a). Clearly, only one peak of electron density was observable along the propagation direction. The peak electron density decreases along with the filament propagation due to the energy loss of laser pulse. The peak electron density was less than the critical electron density ($N_{cr} = 1.8 \times 10^{21}$ cm^{-3}),[27,28] which means that no visible damage was observed after pump pulses irradiation.

Propagation of the filament induced by the first pump pulse along the laser propagation direction was easily observable. However, no similar filament induced by the second pump pulse followed the one induced by the first pump pulse when the pulses propagated deeper into the sample. Instead, two following shallow filaments, on either side of the first one, were observed with high transmissivity. This indicates that the second pump pulse was split. As shown in Fig. 2(b), this phenomenon can be attributed to the fact that the high-reflective surface plasma, induced by the first pump pulse, reshaped the second pump pulse. Due to the Gaussian distribution of the laser pulse, the electron density of the focus center, induced by the first pulse, was higher than the pericentral region. Thus, the reflectivity of the focus center on the surface was higher than that of the pericentral region. When the second pump pulse arrived, the center energy of the second pulse would be most reflected. The pericentral part of the second pulse entered the sample. However, the strong nonlinear effect caused by the ring-shaped electromagnetic field will distort the symmetry of original field distribution,[29] which will further lead to plasma filament split. To further support this explanation, the surface reflectivity at t = 200 fs was calculated by using the plasma model.[28] The simulation result was plotted as Fig. 2(c). As expected,

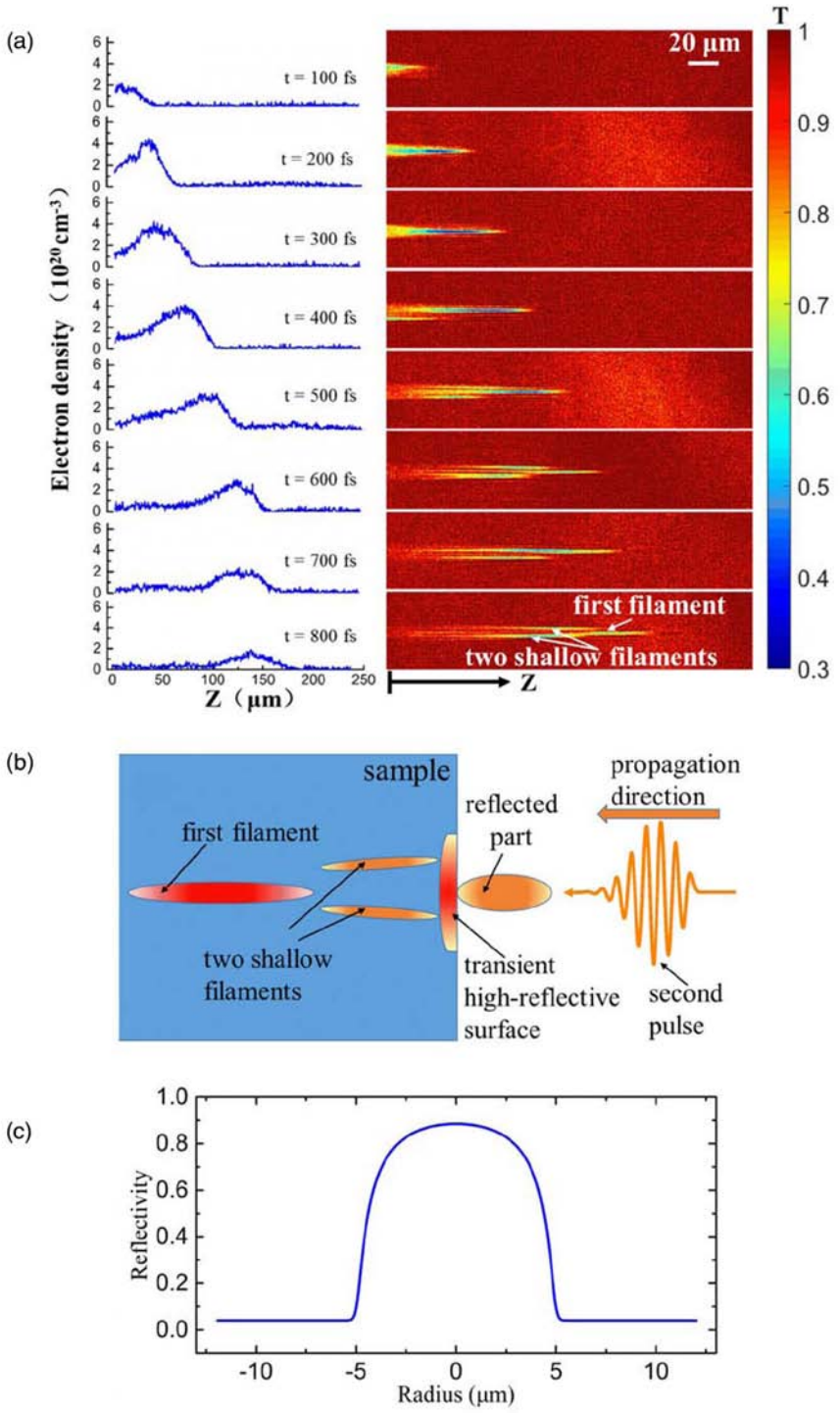

Fig. 2. (a) Two-dimensional transmission mapping and electron density evolution in the center of filaments induced by double pulses with ts = 200 fs. The energy of both pulses is 4 μJ. T denotes the transmissivity. (b) Diagram of filament split caused by the high-reflective surface induced by the first pulse. (c) Instantaneous reflectivity of the surface at t = 200 fs delay from simulation.

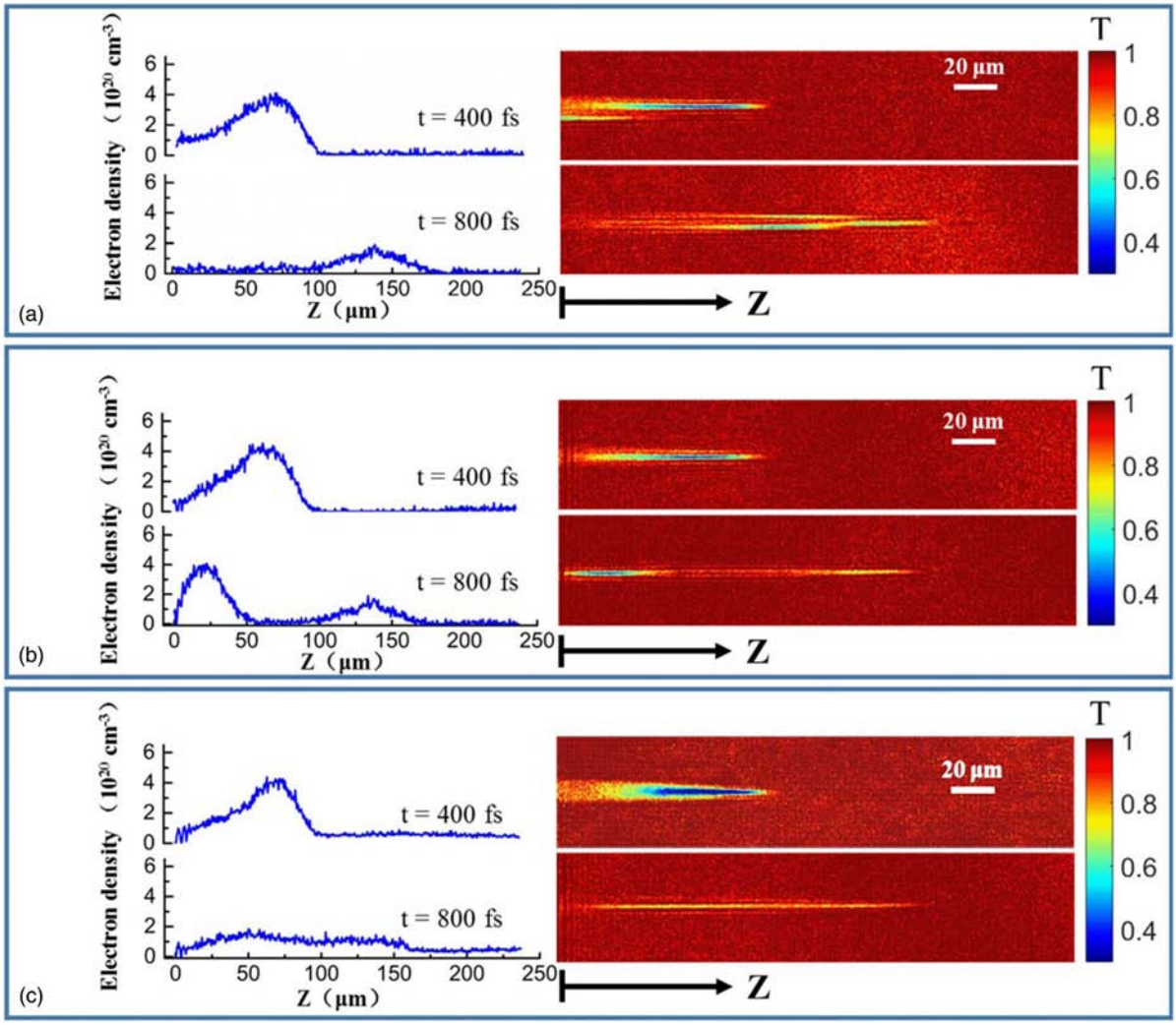

Fig. 3. Comparison of electron density distribution in the center of the filaments after irradiation by (a) 200 fs separation double pulses, (b) 600 fs separation double pulses and (c) single pulse. The energy of the single pulse was 8 μJ, and the energy of each pump pulse in (a) and (b) was 4μJ. T denotes the transmissivity.

the reflectivity at the center of the pulse exceeded 0.8, which strongly reflected the second pulse. However, the reflectivity decreased rapidly in the pericentral area of the pulse. This enabled the second pulse to enter the sample and induce two shallow filaments.

In order to investigate the influence of separation time in double pulses excitation, two separation times (t_s=200 fs and t_s=600 fs) of double pulses cases and single pulse case were employed for comparison, as shown in Fig. 3. In addition, two delay time snapshots (i.e., t=400 fs and t=800 fs) were selected, and the related electron density distribution of the filament center

was plotted. The peak electron density in (a) and (b) was induced by the first subpulse with energy of 4 μJ. However, the peak electron density in (c) was induced by the single pulse with energy of 8 μJ. At t=400 fs, the electron density distribution curves of the filament center in (a)–(c) were similar, and the electron density peaks were all approximately 4×10^{20} cm^{-3}. The same peak density of (a)–(c) is in agreement with the saturation effect in laser induced filaments,[30] which is caused by the nonlinear optical Kerr effect and plasma defocusing.[31,32] At a delay of 800 fs, the electron density distribution of the filaments in the three cases was clearly different. The split filaments in (a) at t=800 fs can be easily observed. By contrast, a second peak density in the center of the filament can be seen in (b), but no split filaments appear. In the single pulse case shown in (c), the electron density relaxed to a low level. The second density peak in (b) is particularly notable. Because the separation time (t_s) between the two pump subpulses in (b) was 600 fs, longer than the 200 fs in case (a), the electron density induced by the first pump subpulse had sufficient time to relax to a lower level before the second subpulse arrived. According to the Drude model,[27] the reflectivity of the focus center on the surface also recovers to a low level with decreasing electron density. Thus, the energy of the second pump subpulse entered the bulk of the sample and induced the second electron density peak. This phenomenon potentially enables control of the energy coupling mode when temporally shaped pulses are applied.

In addition to the electron density distribution at the filament center, the electron dynamics near the center should also be considered. Figure 4 shows the spatial electron density distribution. The 2D electron density distribution was calculated and is color mapped in Figs. 4(b) and 4(c) for double pump pulses and single pulse, respectively. The probe delay time was t = 600 fs. The electron distribution is corresponding to the transmissivity map in Fig. 2. Three electron density peaks, which can be seen in Fig. 4(b), occurred when the second pump pulse was split by the surface plasma induced by the first pulse. The electron distribution 4 μm from the filament center in (b) and (c) is plotted and compared in Fig. 4(a). The electron density near the filament center is higher for the double pulses excitation than for the single pulse excitation. This means that the laser energy was deposited into a broader region when applying the double pump pulses, which is expected to lead to more defects in the large area of the sample. Furthermore, the laser induced defect is helpful to improve subsequent treatments, such as chemical etching.[32]

Electron plasma that is induced by laser pulses stores deposition energy from laser pulses, which is then transported to the lattice.[27–30] Every bound electron in valence band requires the same energy (bandgap) to be excited to conduction band. Therefore, the free electron density can represent the

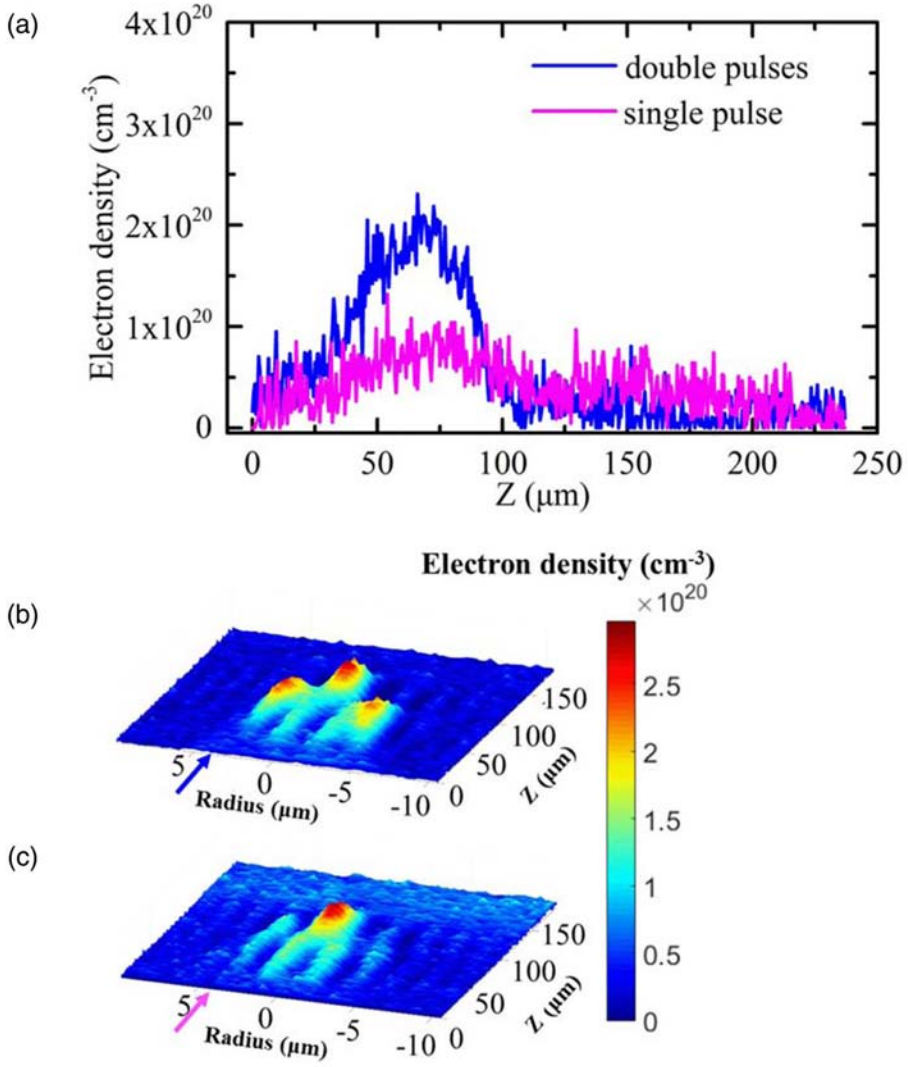

Fig. 4. Spatial electron density distribution of the filaments. The electron density distribution at the position r = 4 μm is plotted in (a) both for double pulses and single pulse. The 2D distribution of the electron density are presented for (b) double pulse and (c) single pulse. The probe delay time was t = 600 fs. The blue and pink arrows in (b) and (c) indicate the positions selected to plot the electron density curve in (a).

amount of deposition energy. For the intensity saturation effect of a filament, the peak intensity of the filament ranges from 10^{13} to 10^{14} Wcm^{-2}.[33] At an intensity of 6×10^{13} Wcm^{-2}, the peak electron temperature attained at the peak of pulse intensity was measured as approximately 22 eV for fused silica.[34] In the first stage of excitation, the electron temperature is unexpected to change much. Thus, it is reasonable to estimate the deposition energy by the total amount of excited electrons. Figure 5 shows a comparison of

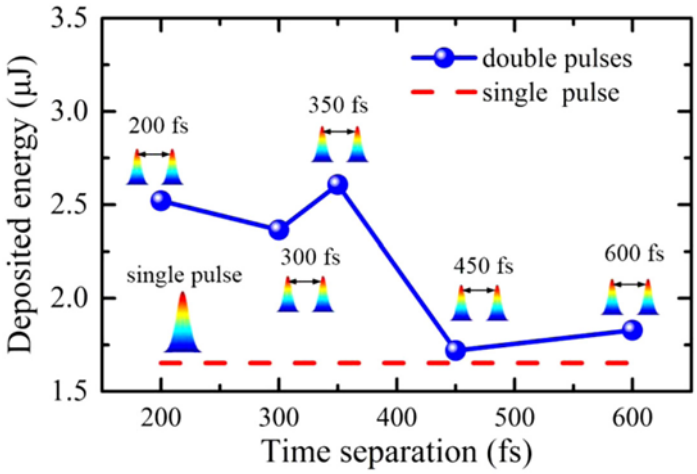

Fig. 5. Deposited energy of double pump pulses with different time separation and single pulses.

the deposition energy among double pump pulses with different separation times and single pulse. All data in the figure were based on the spatial integral of the maximum electron density extracted from all probe delay times. As seen in Fig. 5, the deposition energy of the double pump pulses was generally higher than that of the single pulse. For the double pump pulses, the deposition energy was dependent on the separation time. The maximum deposited energy was obtained at a separation time of 350 fs, which is consistent with the results of laser enhanced chemical etching.[35] However, the deposition energy at a separation time of 450 fs was slightly higher than for the single pulse case. This indicates that we can optimize the deposition energy by tuning the temporal shape of femtosecond laser pulses, which provides a useful method to improve the energy deposition efficiency.

In conclusion, we used double pump pulses to excite wide bandgap material (fused silica) by using the pump–probe technique, and we analyzed the energy deposition and electron dynamics evolution at a high temporal and spatial resolution. We observed that, in the double pump pulses regime, the second pulse was strongly reshaped due to the emergence of a transient high-reflective surface induced by the first pump pulse. Hence, the filament induced by the second pulse was split into two shallow filaments. This splitting phenomenon did not occur when the separation time of the double pulses became larger for the transient high-reflective surface relaxed to a lower electron density. The electron density distribution was analyzed both in and near the center of the filament, which revealed a higher electron density near the center of the filament for the double pump pulses than for the single pulse. This indicated that the energy of the laser pulse was deposited over a larger area of the sample. Total deposition energy was also

estimated and compared among double pump pulses with different separation times and single pulse. Higher efficiency energy deposition was revealed in the double pump pulses regime and the efficiency was strongly dependent on the separation time. This study provides valuable findings regarding wide bandgap material excitation with temporally shaped femtosecond laser pulses and can aid in the understanding of the mechanisms involved in shaped pulse induced energy deposition.

Acknowledgments — This research was supported by the National Key R&D Program of China (Grant No. 2017YFB1104300) and National Natural Science Foundation of China (Grant No. 11704028).

References

1. F. Chen and J. R. V. de Aldana, *Laser Photonics Rev.* 8, 251 (2014).
2. V. Bharadwaj, A. Courvoisier, T. T. Fernandez, R. Ramponi, G. Galzerano, J. Nunn, M. J. Booth, R. Osellame, S. M. Eaton, and P. S. Salter, *Opt. Lett.* 42, 3451 (2017).
3. I. Dey et al., *Nat. Commun.* 8, 1184 (2017).
4. T. Morimoto, N. Sono, T. Miyamoto, N. Kida, and H. Okamoto, *Appl. Phys. Express* 10, 122701 (2017).
5. Y. Minami, H. Yamaki, I. Katayama, and J. Takeda, *Appl. Phys. Express* 7, 022402 (2014).
6. E. Ertorer, M. Haque, J. Li, and P. R. Herman, *Opt. Express* 26, 9323 (2018).
7. S. Ahn, J. Choi, J. Noh, and S.-H. Cho, *Opt. Lasers Eng.* 101, 85 (2018).
8. A. Murata, Y. Shimotsuma, M. Sakakura, and K. Miura, *J. Laser Micro/Nanoeng.* 11, 95 (2016).
9. Y. Li, W. Watanabe, T. Tamaki, J. Nishii, and K. Itoh, *Jpn. J. Appl. Phys*. 44, 5014 (2005).
10. K. Yamada, W. Watanabe, K. Kintaka, J. Nishii, and K. Itoh, *Jpn. J. Appl. Phys.* 42, 6916 (2003).
11. H. R. Lange, A. Chiron, J.-F. Ripoche, A. Mysyrowicz, P. Breger, and P. Agostini, *Phys. Rev. Lett.* 81, 1611 (1998).
12. L. Bergé, *Phys. Rev. E* 69.6, 065601 (2004).
13. P. J. Skrodzki, M. Burger, and I. Jovanovic, *Sci. Rep.* 7, 12740 (2017).
14. M. Scheller, M. S. Mills, M.-A. Miri, W. Cheng, J. V. Moloney, M. Kolesik, P. Polynkin, and D. N. Christodoulides, *Nat. Photonics* 8, 297 (2014).
15. J. Schwarz and J.-C. Diels, *Phys. Rev. A* 65, 013806 (2001).
16. O. G. Kosareva, N. A. Panov, N. Akozbek, V. P. Kandidov, Q. Luo, S. A. Hosseini, W. Liu, J.-F. Gravel, G. Roy, and S. L. Chin, *Appl. Phys. B* 82, 111 (2006).
17. J. Papeer, M. Botton, D. Gordon, P. Sprangle, A. Zigler, and Z. Henis, *New J. Phys.* 16, 123046 (2014).

18. L. Jiang, A.-D. Wang, B. Li, T.-H. Cui, and Y.-F. Lu, *Light: Sci. Appl.* 7, 17134 (2018).
19. Z. Wang, L. Jiang, X. Li, A. Wang, Z. Yao, K. Zhang, and Y. Lu, *Opt. Lett.* 43, 98 (2018).
20. J. Hernandez-Rueda, N. Götte, J. Siegel, M. Soccio, B. Zielinski, C. Sarpe, M. Wollenhaupt, T. A. Ezquerra, T. Baumert, and J. Soli, *ACS Appl. Mater. Interfaces* 7, 6613 (2015).
21. S. W. L. Jiang, W. Han, J. Hu, X. Li, Q. Wang, and Y. Lu, *Appl. Phys. Express* 11, 052703 (2018).
22. Y. Shimotsuma, M. Sakakura, P. G. Kazansky, M. Beresna, J. Qiu, K. Miura, and K. Hirao, *Adv. Mater.* 22, 4039 (2010).
23. Z. Wang, B. Zeng, G. Li, H. Xie, W. Chu, F. He, Y. Liao, W. Liu, H. Gao, and Y. Cheng, *Opt. Lett.* 40, 5726 (2015).
24. L. Englert, B. Rethfeld, L. Haag, M. Wollenhaupt, C. Sarpe-Tudoran, and T. Baumert, *Opt. Express* 15, 17855 (2007).
25. I. H. Chowdhury, X. Xu, and A. M. Weiner, *Appl. Phys. Lett.* 86, 151110 (2005).
26. X. L. Mao, S. S. Mao, and R. E. Russo, *Appl. Phys. Lett.* 82, 697 (2003).
27. P. Balling and J. Schou, *Rep. Prog. Phys.* 76, 39 (2013).
28. L. Jiang and H. L. Tsai, *Int. J. Heat Mass Transf.* 48, 487 (2005).
29. C. Xie, V. Jukna, C. Milián, R. Giust, I. Ouadghiri-Idrissil, T. Itina, J. M. Dudley, A. Couairon, and F. Courvoisier, *Sci. Rep.* 5, 8914 (2015).
30. S. S. Mao, F. Quéré, S. Guizard, X. Mao, R. E. Russo, G. Petite, and P. Martin, *Appl. Phys. A* 79, 1695 (2004).
31. L. Sudrie, A. Couairon, M. Franco, B. Lamouroux, B. Prade, S. Tzortzakis, and A. Mysyrowicz, *Phys. Rev. Lett.* 89, 186601 (2002).
32. S. Tzortzakis, L. Sudrie, M. Franco, B. Prade, A. Mysyrowicz, A. Couairon, and L. Bergé, *Phys. Rev. Lett.* 87, 4 (2001).
33. A. Couairon and A. Mysyrowicz, *Phys. Rep.* 441, 47 (2007).
34. C. Quoix, G. Hamoniaux, A. Antonetti, J.-C. Gauthier, J.-P. Geindre, and P. Audebert, *J. Quant. Spectrosc. Radiat. Transf.* 65, 455 (2000).
35. M. Zhao, J. Hu, L. Jiang, K. Zhang, P. Liu, and Y. Lu, *Sci. Rep.* 5, 13202 (2015).